Hindawi Publishing Corporation
International Journal of Photoenergy
Volume 2013, Article ID 830341, 9 pages
http://dx.doi.org/10.1155/2013/830341

Research Article

Composite Energy Storage System with Photovoltaic Power Generation and Uninterruptible Power Supply Function

Jung-Min Kwon

Department of Electrical Engineering, Hanbat National University, Daejeon 305-719, Republic of Korea

Correspondence should be addressed to Jung-Min Kwon; jmkwon@hanbat.ac.kr

Received 9 March 2013; Revised 13 May 2013; Accepted 3 June 2013

Academic Editor: Wayne A. Anderson

A composite energy storage system (CESS) that includes a photovoltaic (PV) power generation and an uninterruptible power supply (UPS) function is proposed. This system has three operating modes, namely, a grid-connected inverter mode, a grid-connected rectifier mode, and an islanding mode. This system is composed of a boost converter, a three-phase inverter/rectifier, a bidirectional DC/DC converter, and thyristor switches. The boost converter extracts maximum power from the PV panels and sends it to the DC-link. The bidirectional DC/DC converter is connected between the battery and the DC-link, which leads to an optimized charging/discharging operation. The three-phase inverter/rectifier transmits the power to and from the grid. Also, it operates as a UPS in the islanding mode. The thyristor switches are used for connecting/disconnecting between the grid and the AC load. A 15 kW prototype is implemented to verify the performance of the proposed system.

1. Introduction

There are several issues involving electric grid. First, power plants that need to be constructed in order to meet the increasing power demand incur construction and environmental costs. Second, the power fluctuation from the distributed generation from the renewable energy source which is mutually independent in nature produces a negative effect on grid voltage and frequency stabilization. Electrical energy storage can solve these issues and can make grid more efficient and reliable. As shown in Figure 1(a), the energy storage system (ESS) accumulates excess energy and discharges it during peak hours. This could reduce power plant usage and strain on transmission and distribution networks. Figure 1(b) shows the PV power output profile with high-frequency power fluctuation. The ESS can compensate the power fluctuation of the renewable energy sources.

To store energy, several methods are used [1–7]. The pumped-storage hydroelectricity stores energy in the form of water, pumped from a lower elevation reservoir to a higher elevation one. At times of low electrical power demand, excess energy is used to pump water into the higher reservoir. On the contrary, at times of high electrical power demand, water is released back into the lower reservoir through a turbine and electrical power is generated. Such dam construction, however, causes environmental pollution. A flywheel is also used for energy storage [1–3]. It is a rotating mass which can store mechanical energy with the high speed of rotation. It has several advantages such as having no toxic components, being insensitive to the number of charge/discharge cycles, having deep discharges, being temperature resistant, being easy charge level monitoring, having high energy density, and having huge allowable maximum output power. However, the high-speed moving parts and the danger to the surroundings in case of malfunction are its disadvantages. Recently, with the battery capacity being significantly increased and the costs being substantially reduced, there are active researches on ESS based on battery [4–7]. Several methods have been proposed to store the PV energy to the battery as well [8, 9].

The ESS has an inverter because it has to be connected to the grid. It also has a bidirectional converter for battery charging and discharging. The hardware of the ESS is very similar to the uninterrupted power supply (UPS) and the grid connected renewable power generation system [10–12]. Therefore, these three systems can be integrated to one. In this paper, composite energy storage system (CESS) that includes a photovoltaic (PV) power generation and the UPS function

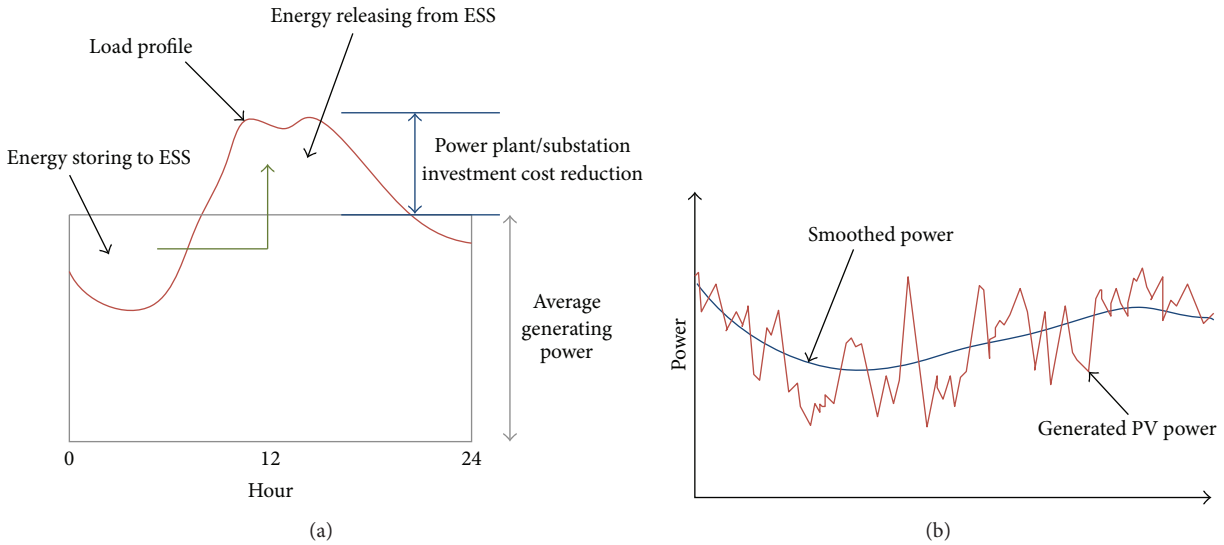

Figure 1: Power curves of ESS and PV systems; (a) power curves of ESS; (b) power curves of PV system.

and its control scheme are proposed. A 15 kW prototype is implemented to verify the performance of the proposed CESS.

2. System Description

Figure 2 shows the configuration of the proposed composite ESS. The proposed CESS is composed of a boost converter, a three-phase inverter/rectifier, a bidirectional converter, and thyristor switches. The boost converter performs the maximum power point tracking (MPPT) control and extracts the maximum power from PV panels and sends it to the DC-link. The bidirectional converter is connected between the battery and the DC-link, which leads to an optimized charging/discharging operation. The bidirectional converter operates as a buck converter which charges the battery and it operates as a boost converter which discharges the battery.

Three-phase AC sources of the grids g_a, g_b, and g_c are connected to the inverter/rectifier and AC load through the thyristor switches. The three-phase converter/rectifier operates as a rectifier or an inverter. It gets the power from the grid or provides the power to the grid and AC load. When it operates as a rectifier, it regulates the voltage across the DC-link capacitors C_{d1} and C_{d2} with a power factor correction (PFC). On the contrary, when it operates as the grid-connected inverter, it provides three-phase sinusoidal output power to the grid and the load with a unity power factor. When the grid has fault, the thyristor switches are turned off and the grid is disconnected between the AC load and the inverter. In this case, the inverter converts the DC-link voltage V_{Cd} into the three sinusoidal output voltages as a UPS. Since the three-phase four-wire inverter is adopted, each phase voltage can be independently controlled to operate well even for an unbalanced AC load.

3. Control Scheme

3.1. Power Flow Control. This system has three operating modes, namely, a grid-connected inverter mode, a grid-connected rectifier mode, and an islanding mode.

(1) Grid-Connected Inverter Mode. The three-phase inverter/rectifier operates as the inverter and it provides the power to the grid and the AC load. The boost converter performs the MPPT control and extracts the maximum power from PV panels and sends it to the DC-link. The battery is charged or discharged according to the balance between the PV power P_{PV} and the output power of the inverter/rectifier P_o. The discharging battery power is

$$P_{bat} = P_{PV} - P_o. \quad (1)$$

If P_{PV} is higher than P_o, the battery is charged; otherwise the battery is discharged.

(2) Grid-Connected Rectifier Mode. The three-phase inverter/rectifier operates as a rectifier and it receives the power from the grid. The boost converter performs the MPPT control and extracts the maximum power from the PV panels and sends it to the DC-link. The battery charging power is

$$-P_{bat} = P_{PV} + P_i, \quad (2)$$

where P_i $(= -P_o)$ is input power of the inverter/rectifier from the grid. If the sum of the PV power and the input inverter/rectifier power is higher than the maximum battery charging power $(-P_{bat,max} < P_{PV} + P_i)$, the mode changes to the grid-connected inverter mode.

(3) Islanding Mode. The CESS operates in this mode when the grid has problems. Table 1 shows the operation in this mode.

(1) $P_{PV} > P_o$ and $P_{PV} < (-P_{bat,max}) + P_o$: in this condition, the boost converter performs the MPPT control and extracts the maximum power from PV panels and sends it to the DC-link. The inverter provides the power to the AC load. The DC-link voltage is regulated by the bidirectional converter. The battery is charged.

(2) $P_{PV} > P_o$, $P_{PV} > (-P_{bat,max}) + P_o$: in this condition, the DC-link voltage is regulated by the boost converters

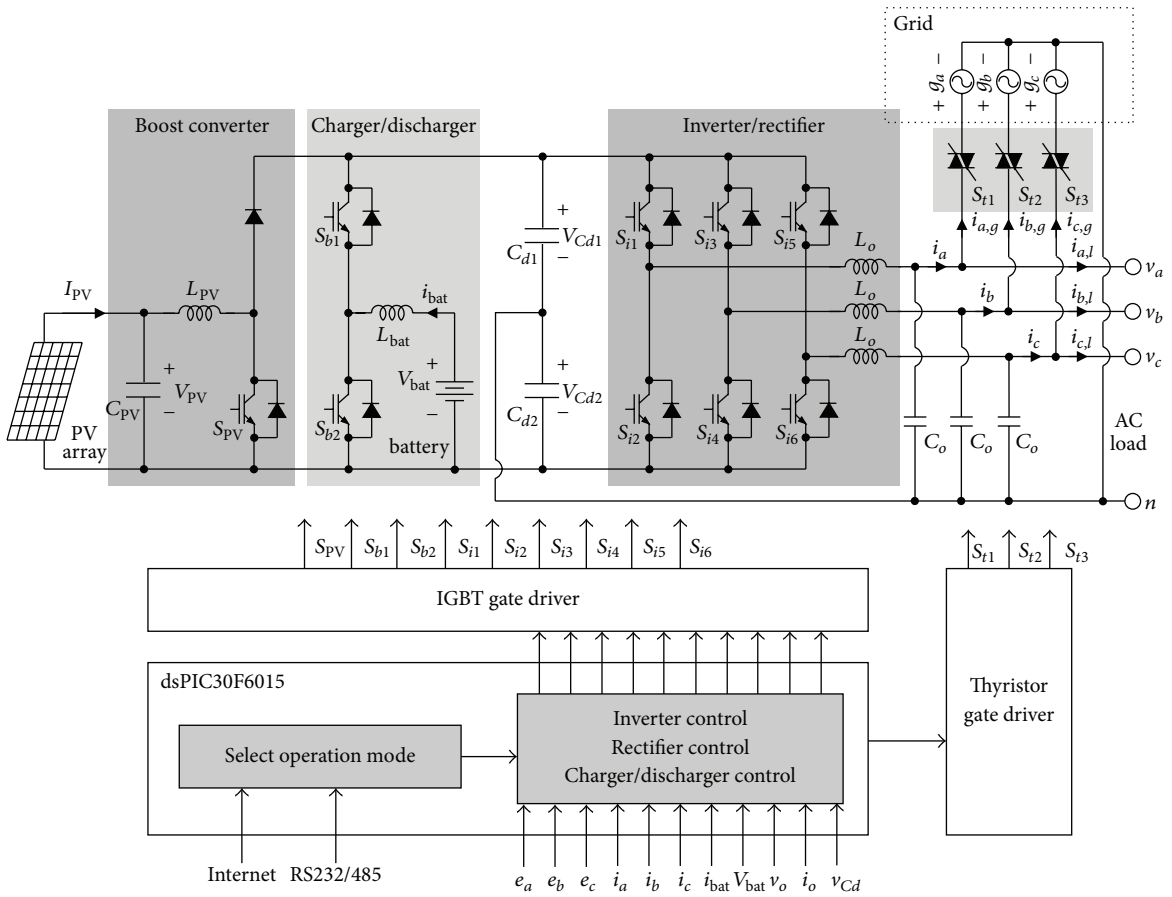

Figure 2: Configuration of the proposed CESS with PV power generation and UPS function.

Table 1: Operation condition in islanding mode.

Condition	Control	
	Boost converter	Bidirectional converter
(1) $P_{PV} > P_o$, $P_{PV} < (-P_{bat,max}) + P_o$	MPPT	V_{Cd} regulation
(2) $P_{PV} > P_o$, $P_{PV} > (-P_{bat,max}) + P_o$	V_{Cd} regulation	Battery charging
(3) $P_{PV} < P_o$	MPPT	V_{Cd} regulation

for the PV panel. Since the maximum power of the PV arrays in this mode is greater than the sum of the AC load demands and the maximum battery charge power $-P_{bat,max}$, the boost converter operates with constant voltage (CV) control. In this case, the battery is charged fully, and the bidirectional converter does not work.

(3) $P_{PV} < P_o$: in this condition, the boost converter performs the MPPT control and extracts maximum power from the PV panels and sends it to the DC-link. The inverter provides the power to AC load. The bidirectional converter discharges the battery and regulates the DC-link voltage by supplying the power $(P_o - P_{PV})$.

3.2. MPPT Control. In order to extract the maximum possible power from the PV panel, the MPPT control is essential. Various MPPT control methods have been proposed, such as a look-up table method, an incremental conductance (IC) method, and a perturb-and-observe (P&O) method. The look-up table method requires prior examination of the PV panel characteristics. However, the PV panel characteristics depend on many complex factors, such as temperature, aging, and the possible breakdown of individual cells. Therefore, it is difficult to record and store all possible system conditions [13, 14]. In contrast, the IC method and the P&O method have an advantage of not requiring solar panel characteristics. The IC method uses the PV panel's incremental conductance dI/dV. At the MPP, it utilizes an expression derived from the condition $dP/dV = 0$. This method provides good performance under rapidly changing conditions [15, 16]. The P&O method perturbs the operating voltage of the PV panel in order to find the direction change for maximized power. When power increases, then the operating voltage is further perturbed in the same direction, whereas when it decreases, then the direction of operating voltage perturbation is reversed [17, 18].

In the proposed system, the modified P&O is utilized [19]. Its flowchart is shown in Figure 3. At the start of the flow chart cycle, the PV voltages V_{PV} and current I_{PV} are sensed and the

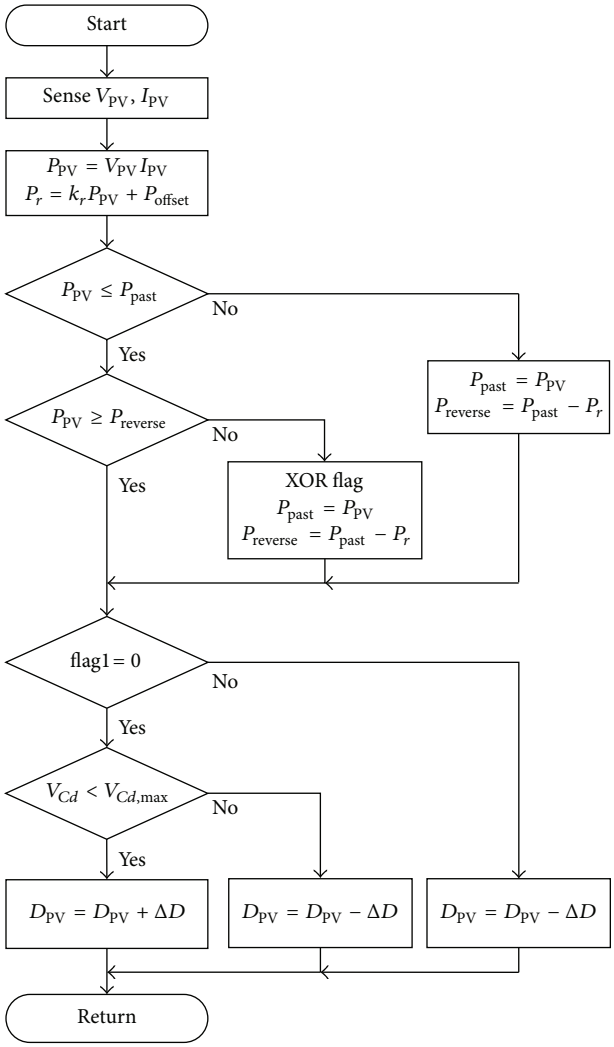

FIGURE 3: Flowchart of adopted MPPT control.

PV power P_{PV} and the permissible perturbing power ripple P_r are calculated. If P_r is too small, the MPPT control becomes very sensitive and can be easily disturbed by measurement errors. In contrast, if P_r is too large, the MPPT efficiency is low at a low insolation. To overcome this problem, P_r is set relative to the PV power as

$$P_r = k_r P_{PV} + P_{offset}, \tag{3}$$

where k_r is a proportional coefficient and P_{offset} is an offset value. The comparative power $P_{reverse}$ for the MPPT direction has a hysteresis characteristic considering the perturbing power ripple P_r as follows:

$$P_{reverse} = P_{past} - P_r, \tag{4}$$

where P_{past} is the PV power updated at the previous cycle. If the existing measurement errors are not greater than P_r, the MPPT direction remains unchanged. The *flag* denotes the duty direction for MPPT. The PV voltage V_{PV} decreases when the flag is 0 and increases when the *flag* is 1. If the following condition is satisfied in the islanding mode:

$$P_{PV} > (-P_{b,max}) - P_o, \tag{5}$$

the DC-link voltage V_{Cd} will increase. If the DC-link voltage V_{Cd} is higher than the maximum DC-link voltage $V_{Cd,max}$, the duty ratio D_{PV} of the boost converter is decreased to reduce the DC-link voltage V_{Cd}.

3.3. Inverter/Rectifier Control in the Grid Connected Modes. Figure 4 shows a control-block diagram of the inverter/rectifier in the grid-connected inverter and rectifier modes. Each phase current is independently controlled. The three-phase inverter/rectifier can be considered as three single-phase half-bridge inverters/rectifiers operating in parallel. Two switches of each leg are driven complementarily with pulse width modulation. In this paper, the analyses of *b*- and *c*-phases are omitted since they are similar to the analysis of the *a*-phase.

When the switch S_{i1} is turned on, the voltage equation is obtained as

$$L_o \frac{d}{dt} i_a = V_{Cd1} - g_a, \tag{6}$$

where i_a is an *a*-phase current and L_o is an inductor of the inverter/rectifier. Similarly, while the switch S_1 is turned off, the voltage equation is obtained as

$$L_o \frac{d}{dt} i_a = -V_{Cd2} - g_a. \tag{7}$$

Depending on a duty ratio D_{i1} of the switch S_{i1}, the average inductor voltage over a switching period T_s gives the *a*-phase current variation Δi_a as follows:

$$L_o \frac{\Delta i_a}{T_s} = (V_{Cd1} - g_a) D_{i1} + (-V_{Cd2} - g_a)(1 - D_{i1}). \tag{8}$$

Therefore, the duty ratio D_{i1} is represented by

$$D_{i1} = D_{i,n} + D_{i,c} = 0.5 + \frac{g_a}{V_{Cd}} + \frac{L_o}{V_{Cd} T_s} \Delta i_a, \tag{9}$$

where the nominal duty $D_{i,n}$ and the controlled duty $D_{i,c}$ are represented as

$$D_{i,n} = 0.5 + \frac{G_a}{V_{Cd}} \sin \omega t,$$
$$D_{i,c} = \frac{L_o}{V_{Cd} T_s} \Delta i_a, \tag{10}$$

where G_a is a peak voltage of g_a and ω is the angular frequency. To force the current i_a of the rectifier to track its current command $i_{a,ref}$, a proportional and integral (PI) current controller is utilized as follows:

$$D_{i,c} = k_p (i_{a,ref} - i_a) + k_i \int (i_{a,ref} - i_a)\, dt. \tag{11}$$

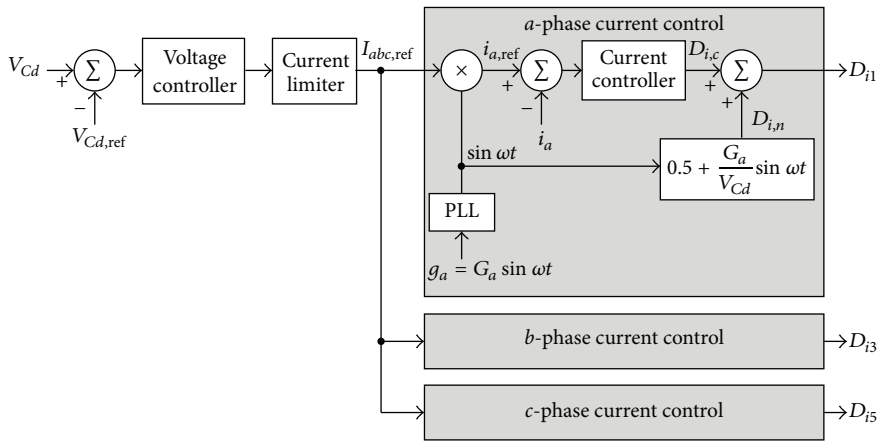

Figure 4: Control-block diagram of the inverter/rectifier at the grid-connected inverter and rectifier modes.

The output $D_{i,c}$ of the current controller only generates the inductor voltage drop required to maintain the sinusoidal current. With the addition of the nominal duty $D_{i,n}$ to the rectifier, which is originally a nonlinear dynamic system, the relation between $D_{i,c}$ and i_a of the inverter/rectifier becomes a first-order linear dynamic system (10) with easy controllability. Thus, the addition of $D_{i,n}$ relaxes the burden of the current controller and improves the input current waveform.

The reference current $I_{abc,\text{ref}}$ has a positive value when the DC-link voltage V_{Cd} is higher than the reference DC-link voltage $V_{Cd,\text{ref}}$. In this case, the CESS operates in the grid-connected inverter mode. The reference current $I_{abc,\text{ref}}$ has negative value when the DC-link voltage V_{Cd} is lower than the reference DC-link voltage $V_{Cd,\text{ref}}$. In this case, the CESS operates in the grid-connected rectifier mode. When the fault is detected from the utility such as a voltage/frequency tolerance or islanding, thyristor switches are turned off and the grid is disconnected between the AC load and the inverter. And the operating mode is changed to the islanding mode.

3.4. Inverter Control in the Islanding Mode. Figure 5 shows the control block diagram of the inverter at the islanding mode. As shown in Figure 5, each phase voltage is independently controlled to operate well even in an unbalanced AC load. The analysis for a-phase voltage is described and others are not described, since the analyses for others are analogous. The duty of the a-phase inverter switch S_{i1} is determined as

$$D_{i1} = 0.5 + m_a \cdot \frac{V_{Cd,\text{ref}}}{V_{Cd}} \sin \omega t, \tag{12}$$

where m_a is the output of the PI voltage controller and $\sin \omega t$ is the reference sine value obtained from a look up table. S_{i2} is driven complementarily with S_{i1}. When the grid-connected mode or when the blackout power is recovered during the islanding mode, $\sin \omega t$ is synchronized with the grid voltage to ensure a smooth transfer of power to the load without a break when the mode is changed.

Protecting the inverter from the overcurrent conditions and still maintaining a reliable power supply to critical loads

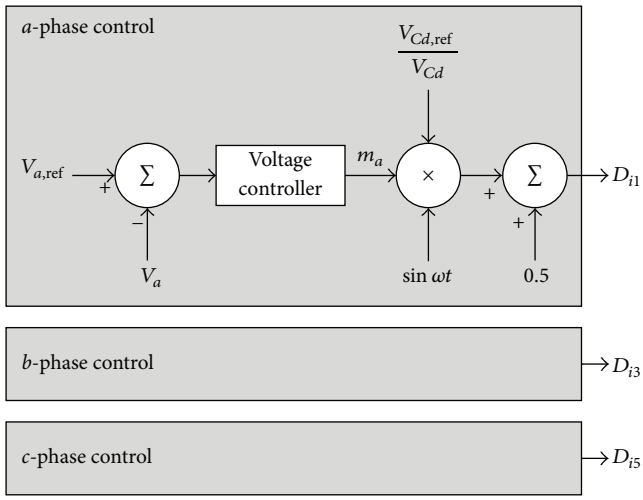

Figure 5: Control-block diagram of the inverter at islanding mode.

are important for UPS [20, 21]. The full-bridge rectifier with capacitive output filter is the most common type of a nonlinear load. When the impulsive load such as a capacitive load is attached, a large current spike affects the switching device. To limit the current spike, the output voltage is forced to have amplitude close to the capacitor voltage of the load when the capacitor load is fully charged [20, 21].

When the grid is back to normal and synchronism is achieved, thyristor switches are turned on and the grid is connected with the AC load and the inverter/rectifier. And the operating mode is changed to the grid-connected inverter or rectifier mode.

3.5. Bidirectional Converter Control. When the battery is discharged, the switch S_{b1} is consistently turned off and the bidirectional converter operates as the boost converter. When the switch S_{b2} is turned on, the voltage equation is obtained as follows:

$$L_{\text{bat}} \frac{di_{\text{bat}}}{dt} = V_{\text{bat}}, \tag{13}$$

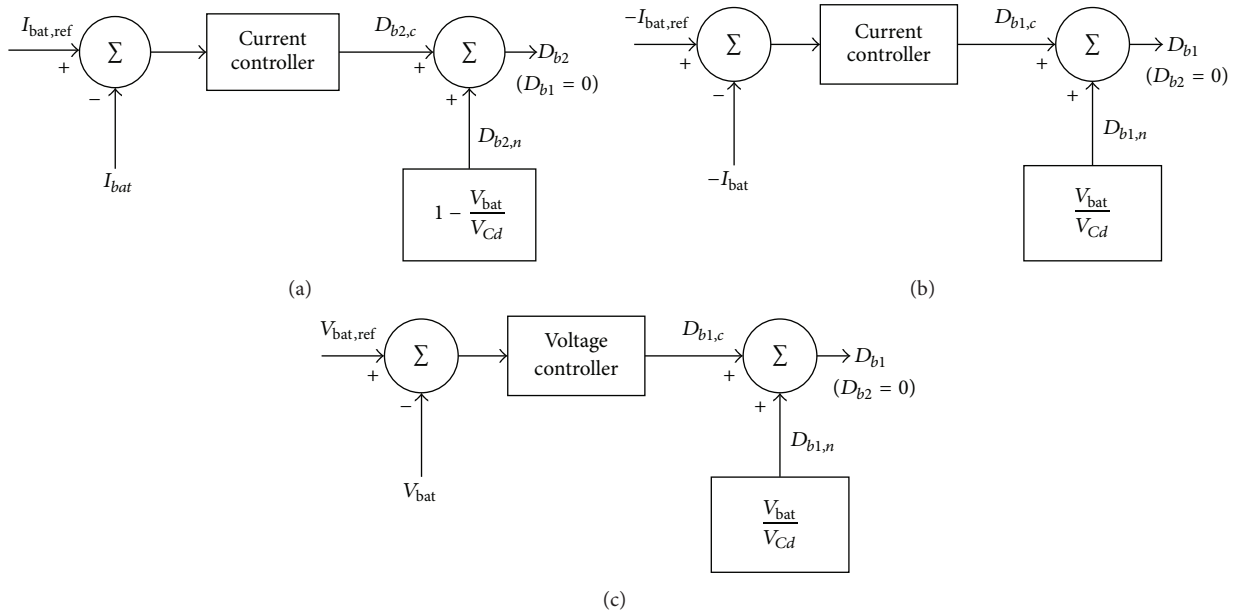

FIGURE 6: Control-block diagrams of the battery charger/discharger; (a) battery discharging control; (b) battery charging control with current control; (c) battery charging control with voltage control.

where i_{bat} is an inductor current flowing into the battery. On the other hand, when the switch S_{b2} is turned off, i_{bat} flows through the body diode of the switch S_{b1}. Thus, the voltage equation is obtained as

$$L_{bat}\frac{di_{bat}}{dt} = V_{bat} - V_{Cd}. \tag{14}$$

Depending on the duty ratio D_{b2} of the switch S_{b2}, the average voltage of the inductor L_{bat} over a switching period T_s (= $1/f_s$) is given as follows:

$$L_{bat}\frac{\Delta i_{bat}}{T_s} = V_{bat}D_{b2} + (V_{bat} - V_{Cd})(1 - D_{b2}). \tag{15}$$

Let the duty ratio D_{b2} be represented by

$$D_{b2} = D_{b2,n} + D_{b2,c}, \tag{16}$$

which is composed of a nominal duty ratio $D_{b2,n}$ and a controlled duty ratio $D_{b2,c}$. From (13)–(16), the nominal duty ratio $D_{b2,n}$ and the controlled duty ratio $D_{b2,c}$ can be represented as

$$\begin{aligned} D_{b2,n} &= 1 - \frac{V_{bat}}{V_{Cd}}, \\ D_{b2,c} &= \frac{L_{bat}\Delta i_{bat}}{V_{Cd}T_s}. \end{aligned} \tag{17}$$

To force I_{bat} to track its command $I_{bat,ref}$, the PI current controller is utilized as follows:

$$D_{b2,c} = k_p(I_{bat,ref} - I_{bat}) + k_i\int(I_{bat,ref} - I_{bat})\,dt. \tag{18}$$

The control diagram for the discharging control is shown in Figure 6(a).

When the battery is charged, the switch S_{b2} is consistently turned off and the bidirectional converter is operated as the conventional buck converter. Since the voltage equations of the charging mode are analogous to the discharging mode, the detail analyses are omitted. In this mode, the average voltage of the inductor L_{bat} over a switching period T_s is given as follows:

$$L_{bat}\frac{\Delta i_{bat}}{T_s} = (V_{bat} - V_{Cd})D_{b1} + V_{bat}(1 - D_{b1}). \tag{19}$$

The duty ratio D_{b1} is obtained as follows:

$$D_{b1} = D_{b1,n} + D_{b1,c} = \frac{V_{bat}}{V_{Cd}} - \frac{V_{bat}\Delta i_{bat}}{V_{Cd}T_s}. \tag{20}$$

To charge the battery, the current/voltage control is selected. Charging starts by controlling current until the battery has reached the maximum voltage. When the maximum battery voltage is reached, current control is switched into voltage control. At this time, the battery is charged at about 70%~85% of its full capacity. The control diagrams of battery charging control are shown in Figures 6(b) and 6(c).

4. Experimental Results

The hardware circuit of the composite ESS that includes the PV power generation and an UPS function in Figure 2 is implemented. It is divided into two parts: the microcontroller-based control circuit and the power circuit. In the microcontroller-based control system, software flexibility facilitates the development and updating of control algorithms and allows modern control theory to be adopted

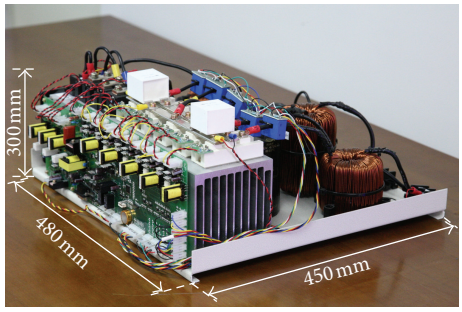

Figure 7: Photograph of 15 kW prototype.

Table 2: Parameters and specifications of the prototype.

Parameters/specifications	Value
Grid voltage	3 phase 380 V
Rated power	15 kW
Switching frequency	15 kHz
PV inductor L_{PV}	1 mH
Battery inductor L_{bat}	1 mH
Output inductors L_o	1.5 mH
DC-link capacitor C_d	2350 μF
PV capacitor C_{PV}	2 μF
Output filter capacitor (C_o)	10 μF

for higher performance. The system is implemented fully in software using a single-chip microcontroller, Microchip dsPIC30F6015. The single-chip microcontroller can implement the controller at a lower cost and a smaller size than a general-purpose microprocessor with accompanying external circuits. The implementation of the voltage and current controllers is performed at every sample period 100 μs. Each MPPT controller is performed at every sample period 100 ms. The 10-bit A/D converter in the microcontroller measures the voltage and current signals. This CESS is designed for the MeOH battery and receives the battery information using RS232/485 communication.

The photograph of the experimental setup of the composite ESS is shown in Figure 7. The thyristor driver board is separated from the main board and the IGBT board. Thus, the AC load can be connected with the grid even if the main board has problems. The selected system parameters are presented in Table 2.

Figure 8 shows the startup behavior of the MPPT control. The MPPT control is started at open circuit voltage point of the PV string (600 V, 0 A). After 50 s, the PV power reaches the maximum PV power point (450 V, 26 A).

Figure 9(a) shows the measured grid voltage and current waveforms at the grid-connected inverter mode. It explicitly shows that the grid current is sinusoidal and in phase with the grid voltage, which implies that only real power is fed to the grid. At the rated power, the grid current produces a near unity power factor (higher than 99%), and its total harmonic distortion (THD) was measured at 2.8%. Additionally, each harmonic component was less than 1.9%. Thus, the THD and harmonic components were kept at low levels, and these also

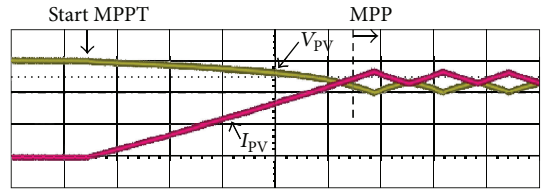

Voltage (200 V/div.), current (10 A/div.), time (10 s/div.)

Figure 8: Startup behavior of the MPPT control.

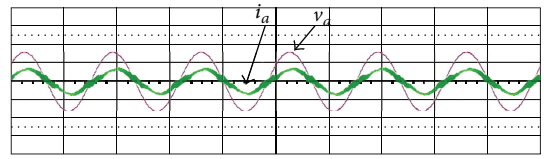

Voltage (200 V/div.), current (10 A/div.), time (10 ms/div.)

(a)

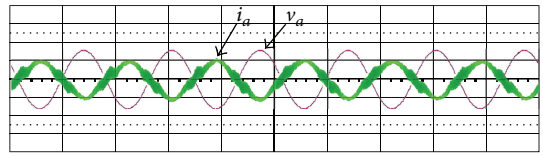

Voltage (200 V/div.), current (10 A/div.), time (10 ms/div.)

(b)

Figure 9: Inverter/rectifier voltage v_a and current i_a; (a) battery discharging; (b) battery charging.

satisfy the following grid current regulation: THD less than 5% and each harmonic component less than 3%. Figure 9(b) shows the measured grid voltage and current waveforms at the grid-connected rectifier mode. The grid current is sinusoidal but there is 180° phase gap. It shows that the current flows to the opposite direction and the composite ESS absorbs the grid power. At this time, the absorbed grid power is stored in the battery.

Figure 10(a) shows the AC load voltages v_{an}, v_{bn}, and v_{cn} and the inverter current i_b when the mode is changed from the islanding mode to the grid-connected inverter mode. The mode is changed without a voltage distortion. At the islanding mode, the current depends on the AC load voltage and the load and it is not being controlled. At the grid-connected modes, the current is controlled to reach the predetermined reference current. Therefore, the current is changed when the mode is changed. Figure 10(b) shows the AC load voltages v_{an}, v_{bn}, and v_{cn} and the AC load current $i_{b,l}$ when the mode is changed from the grid-connected mode to the islanding mode. The mode is changed without a voltage distortion. The AC load current depends on the AC load voltage and the AC load. Since the AC load voltage is not changed, the AC load current is not changed when the mode is changed. At the islanding mode, the THD of the voltage was measured at 2.3% and each harmonic component was less than 1.8%.

5. Conclusion

A composite ESS that includes the PV power generation and the UPS function is proposed. This system has

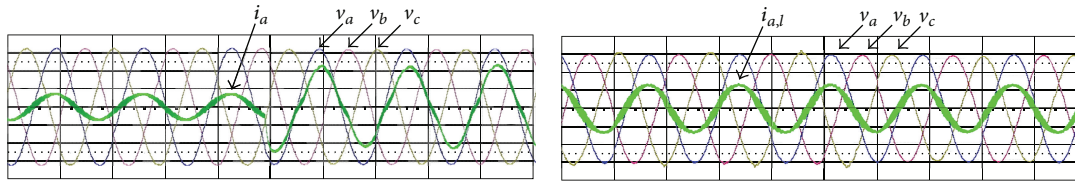

Voltage (100 V/div.), current (10 A/div.), time (10 ms/div.)

(a)

Voltage (100 V/div.), current (5 A/div.), time (10 ms/div.)

(b)

FIGURE 10: Three-phase voltage and current when the mode is changing; (a) AC load voltages v_a, v_b, and v_c and current i_a when the mode is changed from the islanding mode to the grid-connected mode; (b) AC load voltages v_a, v_b, and v_c and AC load current $i_{a,l}$ when the mode is changed from the grid-connected mode to the islanding mode.

three operating modes, namely, the grid-connected inverter mode, the grid-connected rectifier mode, and the islanding mode, and is composed of a boost converter, a three-phase inverter/rectifier, a bidirectional converter, and thyristor switches. The boost converter performs the MPPT control. The three-phase converter/inverter provides the power to the grid or receives the power from the grid when the grid is connected. Also, it operates as the UPS in the islanding mode. The bidirectional converter charges or discharges the battery. The thyristor switches are used for connecting/disconnecting with the grid and the AC load. A 15 kW prototype is implemented to verify the performance of the proposed system.

Acronyms

ESS: Energy storage system
UPS: Uninterrupted power supply
CESS: Composite energy storage system
PV: Photovoltaic
MPPT: Maximum power point tracking
PFC: Power factor correction
CV: Constant voltage
CC: Constant current
IC: Incremental conductance
P&O: Perturb-and-observe
PI: Proportional and integral
THD: Total harmonic distortion.

Acknowledgment

This research was supported by the Basic Science Research Program through the National Research Foundation of Korea (NRF) funded by the Ministry of Education, Science and Technology (NRF-2012R1A1A1003469).

References

[1] W. Keyin, L. Dezhi, M. Jin, O. Yangbin, Z. Xiaofei, and C. Junquan, "Design and simulation of a 12-phase flywheel energy storage generator system with linearly dynamic load," *IEEE Transactions on Applied Superconductivity*, vol. 20, no. 3, pp. 1050–1054, 2010.

[2] J. Lee, S. Jeong, Y. H. Han, and B. J. Park, "Concept of cold energy storage for superconducting flywheel energy storage system," *IEEE Transactions on Applied Superconductivity*, vol. 21, no. 3, pp. 2221–2224, 2011.

[3] M. Subkhan and M. Komori, "New concept for flywheel energy storage system using SMB and PMB," *IEEE Transactions on Applied Superconductivity*, vol. 21, no. 3, pp. 1485–1488, 2011.

[4] Q. Wang and S. S. Choi, "The design of battery energy storage system in a unified power-flow control scheme," *IEEE Transactions on Power Delivery*, vol. 23, no. 2, pp. 1015–1024, 2008.

[5] P. Mercier, R. Cherkaoui, and A. Oudalov, "Optimizing a battery energy storage system for frequency control application in an isolated power system," *IEEE Transactions on Power Systems*, vol. 24, no. 3, pp. 1469–1477, 2009.

[6] H. Qian, J. Zhang, J.-S. Lai, and W. Yu, "A high-efficiency grid-tie battery energy storage system," *IEEE Transactions on Power Electronics*, vol. 26, no. 3, pp. 886–896, 2011.

[7] H. Zhou, T. Bhattacharya, D. Tran, T. S. T. Siew, and A. M. Khambadkone, "Composite energy storage system involving battery and ultracapacitor with dynamic energy management in microgrid applications," *IEEE Transactions on Power Electronics*, vol. 26, no. 3, pp. 923–930, 2011.

[8] L. Liu, H. Li, Z. Wu, and Y. Zhou, "A cascaded photovoltaic system integrating segmented energy storages with self-regulating power allocation control and wide range reactive power compensation," *IEEE Transactions on Power Electronics*, vol. 26, no. 12, pp. 3545–3559, 2011.

[9] K. Sun, L. Zhang, Y. Xing, and J. M. Guerrero, "A distributed control strategy based on DC bus signaling for modular photovoltaic generation systems with battery energy storage," *IEEE Transactions on Power Electronics*, vol. 26, no. 10, pp. 3032–3045, 2011.

[10] W. Sölter, "A new international UPS classification by IEC 62040-3," in *Proceedings of the 24th International Telecomunications Energy Conference (INTELEC '02)*, pp. 541–545, October 2002.

[11] B.-H. Kwon, J.-H. Choi, and T.-W. Kim, "Improved single-phase line-interactive UPS," *IEEE Transactions on Industrial Electronics*, vol. 48, no. 4, pp. 804–811, 2001.

[12] J.-M. Kwon, B.-H. Kwon, and K.-H. Nam, "Three-phase photovoltaic system with three-level boosting MPPT control," *IEEE Transactions on Power Electronics*, vol. 23, no. 5, pp. 2319–2327, 2008.

[13] T. Hiyama, S. Kouzuma, and T. Imakubo, "Identification of optimal operating point of PV modules using neural network for real time maximum power tracking control," *IEEE Transactions on Energy Conversion*, vol. 10, no. 2, pp. 360–367, 1995.

[14] T. Hiyama and K. Kitabayashi, "Neural network based estimation of maximum power generation from PV module using

environmental information," *IEEE Transactions on Energy Conversion*, vol. 12, no. 3, pp. 241–246, 1997.

[15] J.-M. Kwon, K.-H. Nam, and B.-H. Kwon, "Photovoltaic power conditioning system with line connection," *IEEE Transactions on Industrial Electronics*, vol. 53, no. 4, pp. 1048–1054, 2006.

[16] J. H. Lee, H. Bae, and B. H. Cho, "Advanced incremental conductance MPPT algorithm with a variable step size," in *Proceedings of the 12th International Power Electronics and Motion Control Conference (EPE-PEMC '06)*, pp. 603–607, Portorož, Slovenia, September 2006.

[17] J. H. R. Enslin, M. S. Wolf, D. B. Snyman, and W. Swiegers, "Integrated photovoltaic maximum power point tracking converter," *IEEE Transactions on Industrial Electronics*, vol. 44, no. 6, pp. 769–773, 1997.

[18] N. Femia, G. Petrone, G. Spagnuolo, and M. Vitelli, "Optimizing sampling rate of P&O MPPT technique," in *Proceedings of the IEEE 35th Annual Power Electronics Specialists Conferencev (PESC '04)*, pp. 1945–1949, June 2004.

[19] J.-M. Kwon, B.-H. Kwon, and K.-H. Nam, "Grid-connected photovoltaic multistring PCS with PV current variation reduction control," *IEEE Transactions on Industrial Electronics*, vol. 56, no. 11, pp. 4381–4388, 2009.

[20] E.-H. Kim, J.-M. Kwon, J.-K. Park, and B.-H. Kwon, "Practical control implementation of a three- to single-phase online UPS," *IEEE Transactions on Industrial Electronics*, vol. 55, no. 8, pp. 2933–2942, 2008.

[21] E.-H. Kim, J.-M. Kwon, and B.-H. Kwon, "Transformerless three-phase on-line UPS with high performance," *IET Power Electronics*, vol. 2, no. 2, pp. 103–112, 2009.